Simulation of wall erosion in Hall thrusters

IEPC-2007-067

Presented at the 30th International Electric Propulsion Conference, Florence, Italy
September 17-20, 2007

E. Ahedo [*] and A. Antón [†]
Universidad Politécnica de Madrid, Madrid 28040, Spain

I. Garmendia[‡] and I. Caro[§]
Inasmet-Tecnalia, Mikeletegi 2, San Sebastián 20009, Spain

and

J. González del Amo[**]
ESA/ESTEC, Keplerlaan, 1, Noordwijk, The Netherlands.

Wall sputtering of ceramic walls of Hall thrusters is simulated with a two-dimensional hybrid code. The erosion model is based on the volumetric sputtering yield function and the local distributions of ion energy and incidence angle at the wall. The influence of the functional expression of the sputtering yield on erosion is analyzed. Ion properties at impact take into account the presence of Debye sheaths. The influence of different plasma magnitudes on the erosion rate is discussed. The evolution of plasma properties and wall erosion, as the walls get deformed, is calculated for moderate and high discharge voltages. The magnetic field topology has a significant role on erosion too.

I. Introduction

The most important process limiting the lifetime of Hall thrusters is the sputtering of the chamber ceramic walls. by impact of energetic ions. Experimental tests in vacuum chambers of the popular SPT-100[2,21] and PPS-1350[14,34] indicate that their lifetime is in the range 7.000-10.000 hours for nominal conditions (1-1.5kW and ~300V). A reliable knowledge of the actual thruster lifetime and variations of performances along the thruster lifetime is crucial for the good planning of a flight mission and the optimization of the propulsion subsystem. However, laboratory tests of several thousand hours are very expensive in time and resources, and delay painfully the flight certification of the thruster. Furthermore, erosion pattern and thruster lifetime depend on operation conditions (such as discharge voltage, mass flow, and magnetic topology), thruster design, power range, and wall material[4,13,27,30,33,37]. A life test for each operational mode of a thruster is unaffordable.

[*] Professor, Escuela Técnica Superior de Ingenieros Aeronáuticos, eduardo.ahedo@upm.es.
[†] PhD Student, Escuela Técnica Superior de Ingenieros Aeronáuticos, alfredoanton@fmetsia.upm.es.
[‡] Head of Computer Simulation Group, inaki.garmendia@inasmet.es
[§] Head of Functional Materials and Particle Technologies, inaki.caro@inasmet.es
[**] Head of Electric Propulsion Section, José.Gonzalez.del.Amo@esa.int

In this context, reliable simulations of (i) the local plasma conditions at the wall vicinity and (ii) the wall sputtering yield function are of prime importance in order to reduce the number and duration of lifetime tests. Russian researchers have developed accelerated test procedures, constituted of several erosion cycles, each one consisting of three phases: (1) a short period of testing -of the order of 100 hours-, (2) the calculation of the predicted wall wearing during the next ~500-1000 hours from the measurement of the eroded wall profiles, and (3) the mechanical processing of the computed wall profile[1,30,31]. The simulation phase of the wall wearing is based on the estimation of the ion distribution impinging the wall. This distribution is not obtained from the simulation of the plasma discharge in the chamber but from a semi-empirical algorithm where ions are created at one or two point sources and follow a ray motion. The parameters of this ion model are fitted from the measurements of the wall profile made after the experimental phase of each cycle. Obviously, the validation of the algorithm is based only on the comparison of estimated and experimental profiles. The comparison of the SPT-100 wall erosion data with results from this accelerated test procedure shows that it is possible to get an acceptable simulation of the wall final wearing spending a total experimental time of about 10-20% of the targeted thruster operation time[27]. Additional empirical laws are being used in order to avoid a specific test for each operational point of a thruster and for each thruster of the SPT family[27].

The alternative to the above ion-source algorithm is a reliable simulation of the plasma discharge inside the chamber. The advantages of this procedure would be: (1) it is based on a real physical model, (2) it relates the erosion behavior to the plasma response and thruster performances, and (3) it is readily applicable to different thruster designs and powers. Regrettably, there is still much progress to be done in order to have a reliable enough simulation of the plasma discharge.

Two-dimensional(2D), hybrid (i.e. particle/fluid) codes are nowadays the best trade-off in terms of affordability and physical consistency for the simulation of the plasma discharge. This justifies that they are being increasingly used for erosion estimates, as work at the Massachusetts Institute of Technology (MIT)[12], the Joint Propulsion Laboratory[20], and the Universidad Politécnica de Madrid(UPM)[7,15], among others, illustrate. These three centers use for lifetime studies, different versions of the code HPHall-2, developed originally at MIT[18] and updated at UPM[36]. The code is quasineutral except for Debye sheaths tied to the anode and the lateral walls.

This paper reports on simulations of wall sputtering made with an advanced version of HPHall-2[17]on the Centrospazio 5kW thruster (here called CS5) with boron nitride (BN) walls. The geometrical and material data for the simulated thruster was based on data from Ref. 8. The aspects discussed here are: the influence of different forms of the sputtering yield law on the erosion pattern; the evolution of erosion, performances, and plasma characteristics with time; and the influence of the discharge voltage and magnetic field on wall erosion. An Appendix reports on work in-progress for fitting data from SRIM simulations with experimental results.

II. The sputtering yield model

The dependence of the erosion rate on the velocity distribution function of ions, $f_{iW}(\vec{v})$, at a particular wall location is

$$\frac{dh}{dt} = \iiint d^3\vec{v}\; f_{iW}(\vec{v})\; \vec{v}\cdot\vec{n}\; eY_V(E,\theta), \tag{1}$$

where h is the local erosion depth, $\vec{n}$ is the wall normal (Fig.1), $E = mv^2/2$ is the impact energy of ions, θ is the impact angle, and $Y_V(E,\theta)$ is the volumetric sputtering yield, in units of sputtered volume (commonly in mm^3) per 'equivalent' Coulomb. The adjective 'equivalent' is because of experiments for sputtering yield determination give generally $Y_V(E,\theta)$ for a monoenergetic beam of singly-charged ions, whereas neutrals and multiply-charged ions are also present in real conditions. [The volumetric sputtering yield per impacting particle, i.e. $eY_V(E,\theta)$, would not lead to confusions but is rarely used.]

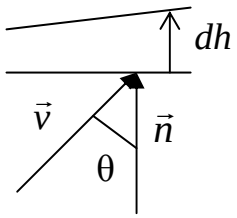

Figure 1: Impact parameters.

In HPHall heavy particles are treated with PIC-MCC methods. Around 10^5 macroparticles, simulating neutrals, singly-charged and doubly-charged ions, are used in our simulations. The adaptation of Eq. (1) to the PIC-based simulation code leads to the following expression for the erosion rate of a wall panel of area ΔA,

$$\frac{dh}{dt} = \frac{1}{\Delta A\, N_{it}\Delta t}\sum_{1}^{N_{it}}\sum_{p} N_p eY_V(E_{pW},\theta_{pW}),$$

where: subscript p and W refer to each heavy particle impacting the wall and the wall location, respectively; $N_p(\sim 10^{10})$ is the number of ions in each (macro)particle; E_p is the energy per ion (not per macroparticle); $\Delta t\,(\sim 10^{-8}\,\mathrm{s})$ is the timestep in the simulation; and $N_{it}(\sim 10^5)$ is the number of iterations in the simulation (so that $t_{sim} = N_{it}\Delta t$ is the simulation time). Related magnitudes of interest are the ion current to the wall

$$j_{iW} = \frac{e}{\Delta A\, N_{it}\Delta t}\sum_{1}^{N_{it}}\sum_{p} Z_p N_p,$$

with Z_p the particle charge number, and the energy flux of heavy species to wall W

$$q_{iW} = \frac{1}{\Delta A\, N_{it}\Delta t}\sum_{1}^{N_{it}}\sum_{p} N_p E_{pW}.$$

Here, the energy at the wall is $E_{pW} = E_{pQ} + eZ_p\phi_{WQ}$, with E_{pQ} the energy at the sheath edge Q (i.e. the boundary of the quasineutral domain of plasma simulations) and ϕ_{WQ} the local potential fall in the Debye sheath. This sheath produces an angular shift of the particle too, with $\theta_W < \theta_Q$, in general. Average values of the ion energy at wall and sheath edge are $\langle E_{pW} \rangle = q_{iW} / g_{iW}$ and $\langle E_{pQ} \rangle = q_{iQ} / g_{iW}$ with q_{iQ} the energy flux at the sheath edge.

A. The sputtering yield law

Published experimental data on $Y_V(E,\theta)$ for Xe^+ impacting on BN and borosil is scarce, mainly in the energy range of interest for Hall thrusters[1,10,22,28]. Figure 2 summarizes the data we have collected for BN and Borosil. It is common (although not exact in practice) to make a variable separation of the sputtering yield law: $Y_V(E,\theta) = Y_O(E)F(\theta)$ with $F(0) = 1$. Notice the large dispersion of data from different experiments and the lack of results for low E. This is going to be an important drawback when computing erosion at the typical discharge voltage of 300V and below. In addition, Abgaryan et al. and Kim et al. use a Hall thruster as the source of impacting ions. This implies that the ion energy at impact is bad known, since only the discharge voltage V_d of the SPT source is given and the beam is not monoenergetic; in Fig. 2 we took $E = 0.80\,V_d$ for these experimental results with a SPT source. Finally, notice that we cannot assure that Fig. 2 is comparing the same material since borosil is a mixture of different proportions of BN and silicon dioxide.

The limitations of the experimental data are overcome by using fitting formulae based on different sputtering theories[9,32]. The theories are generally developed only for monoatomic solids and determine the sputtering yield in terms of sputtered atoms per impacting ion, $Y_A(E,\theta)$ [atom/ion]. The relation with the volumetric sputtering yield is

$$Y_A\left[\text{atoms/ion}\right] = eY_V\left[\text{mm}^3/\text{C}\right] \times N_{Avogrado}[\text{atom/mol}]\,\frac{\rho_t\left[\text{gr/mm}^3\right]}{M_t\left[\text{gr/mol}\right]}$$

with ρ_t and M_t the density and molar mass of the (monoatomic) target.

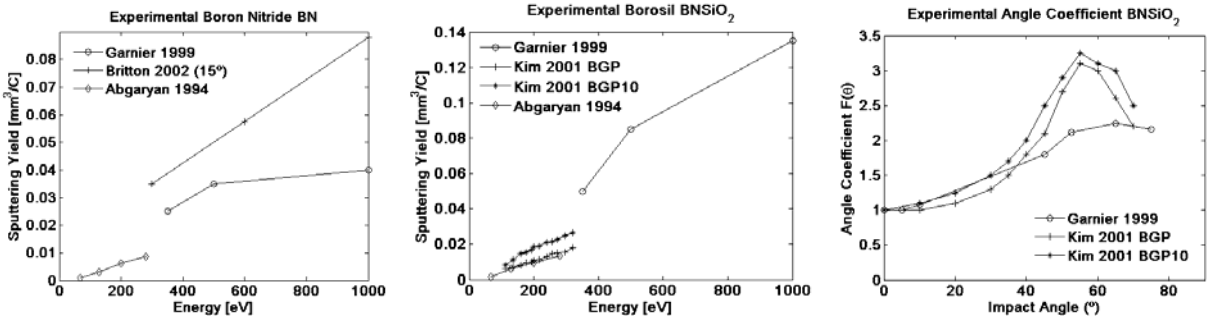

Figure 2: Experimental data on the sputtering yield for erosion by Xe^+: (left) $Y_O(E)$ for boron nitride; (middle) $Y_O(E)$ for borosil; and (right) $F(\theta)$ for borosil.

Perhaps the most relevant set of semi-empirical formulae are those of Yamamura[39,40], valid only for monoatomic solids. The main Yamamura formula for the energy dependence can be expressed as

$$Y_0(E) = S(M_p, M_t, Z_p, Z_t, U_s, E) \times \left(1 - \sqrt{\frac{E_{thr}}{E}}\right)^s, \quad s \sim 2.5 - 2.8$$

where E_{thr} is the threshold energy for sputtering and S is a complex function of the properties of the projectile and the target. In the low-energy range, one has[20] $S \propto E^{1/2}$. Yamamura proposes a single formula for $F(\theta)$ with two empirical parameters. The agreement of the Yamamura formulas with experimental data (for monoatomic targets) is satisfactory for $Y_O(E)$, at the intermediate and large energy ranges. In the low energy range, the data is scarce and no clear conclusion can be extracted on the correctness of the value of E_{thr} and the functional dependence on E. The experimental confirmation of the Yamamura formula for $F(\theta)$ is rather dubious, mainly for heavy projectiles, which suggests that, whenever possible, the direct use of experimental results is preferable.

In composite materials, and in particular with borosil, the sputtering process is more complex[24] and bad known. The extension of the Yamamura formalism to composite materials can be postulated but certainly it has not been proven. However there exists no alternative formalism for the low-energy range of interest for Hall thrusters[9]. Kim[27] suggests that, in the range of discharge voltages of present interest, 200-1000V, $Y_O(E)$ can be fitted to experimental data by a linear function. Kannenberg et al.[25], for erosion of surfaces external to the thruster, take $Y_O(E)$ linear and use a 3rd-order polynomial on $\cos\theta$ for $F(\theta)$. Gamero et al.[20] suggest extending the simplified Yamamura formula

$$Y_0(E) = S_0 \sqrt{E} \left(1 - \sqrt{\frac{E_{thr}}{E}}\right)^{2.5}$$

to composite materials, by adjusting parameters S_0 and E_{thr} empirically from experimental data, and to use a 3rd order polynomial on $\cos\theta$ for $F(\theta)$. Abgaryan et al. propose to take $Y_O(E) \propto E^{5/3}$ for $E < 80$eV (thus setting E_{thr} =0). The attempt to fit experimental data with TRIM/SRIM simulations is reported in the Appendix.

III. Influence of the sputtering yield function

In order to analyze the sensitivity of wall erosion to the functional form of $Y_V(E,\theta) = Y_O(E)F(\theta)$ different laws have been tested with plasma simulations with the CS5 thruster. Figures 3(a) to 3(c) present the erosion profile $h(z)$ of the inner wall of the thruster, operating at 300V and 6mg/s, for different expressions of $Y_O(E)$ and the angular dependence given by

$$F(\theta)=\begin{cases}1+(F_{\max}-1)\exp\left[-a\dfrac{(\theta-\theta_{\max})^2}{\theta_{\max}^2}\right], & \theta<\theta_{\max},\\ F_{\max}\left(1-\dfrac{\pi}{2\theta}\right)\left(\dfrac{1-\theta_{\max}/\theta}{1-2\theta_{\max}/\pi}\right)^2, & \theta>\theta_{\max},\end{cases}$$

with $\theta_{\max}$ the angle that maximizes $F(\theta)$, $F_{\max}=F(\theta_{\max})$, and a a fitting parameter. This expression adjusts very well the experimental data, as Fig. 2 illustrates. In Figs. 3(a) and 3(c), we take $Y_O(E)$ linear,

$$Y_O(E)=c\times\begin{cases}0, & E<E_{th}\\ E-E_{th}, & E>E_{th}\end{cases},$$

with the slope c a constant. Notice that the total erosion is proportional to the operation time and c:

$$h(z)=t_{oper}\frac{dh}{dt}\propto t_{oper}c\,.$$

Since here we are interested in the comparison of different laws for $Y_V(E,\theta)$, the particular values of t_{oper} and c are unimportant. In Fig. 3(b) $Y_O(E)$ is linear except in the threshold vicinity. The right plots of Figs. 3(a)-3(c), where Δh_{exit} means the increase of the width of the chamber exit cross-section, show changes in the shape of the eroded profiles.

Figure 3(a) illustrates the sensitivity of $h(z)$ to variations (or uncertainties) on the vertical position of the linear law of $Y_O(E)$; notice that the uncertainty is just of a 10% in the range 200-400V, where experimental data exists. The eroded profiles show a large sensitivity to this uncertainty, both in absolute (middle plot) and relative terms (right plot). Figure 3(b) considers the case (b) of Fig. 3(a) except for changes/uncertainties on the behaviour around the energy threshold. The sensitivity of $h(z)$ is still important (for a discharge voltage of 300V), which means that for V_d =300V there are still a large number of ions impacting the walls with relatively low E. Figure 3(c) shows the sensitivity to uncertainties on the location of $\theta_{\max}$. We observe that $h(z)$ increases as $\theta_{\max}$ decreases, but the relative erosion profiles are similar, which has not simple to interpretation.

IV. Evolution of wall erosion with time

This section presents simulations of the CS5 at 300V and 6mg/s. Figure 4 shows the temporal evolution of the chamber erosion. The sputtering yield function corresponds to the case of Fig. 3(a) with E_{th}=60eV. Nine stages (called stages 0 to 8) of the eroded ceramic chamber have been simulated. Each stage corresponds to Δh_{exit}~1mm. Notice in Fig. 4(a) the different shapes of the inner and outer walls (similar asymmetries are observed in other thrusters[33]) and the larger erosion of the inner wall. Figure 4(b) shows the typical decrease of the volumetric erosion

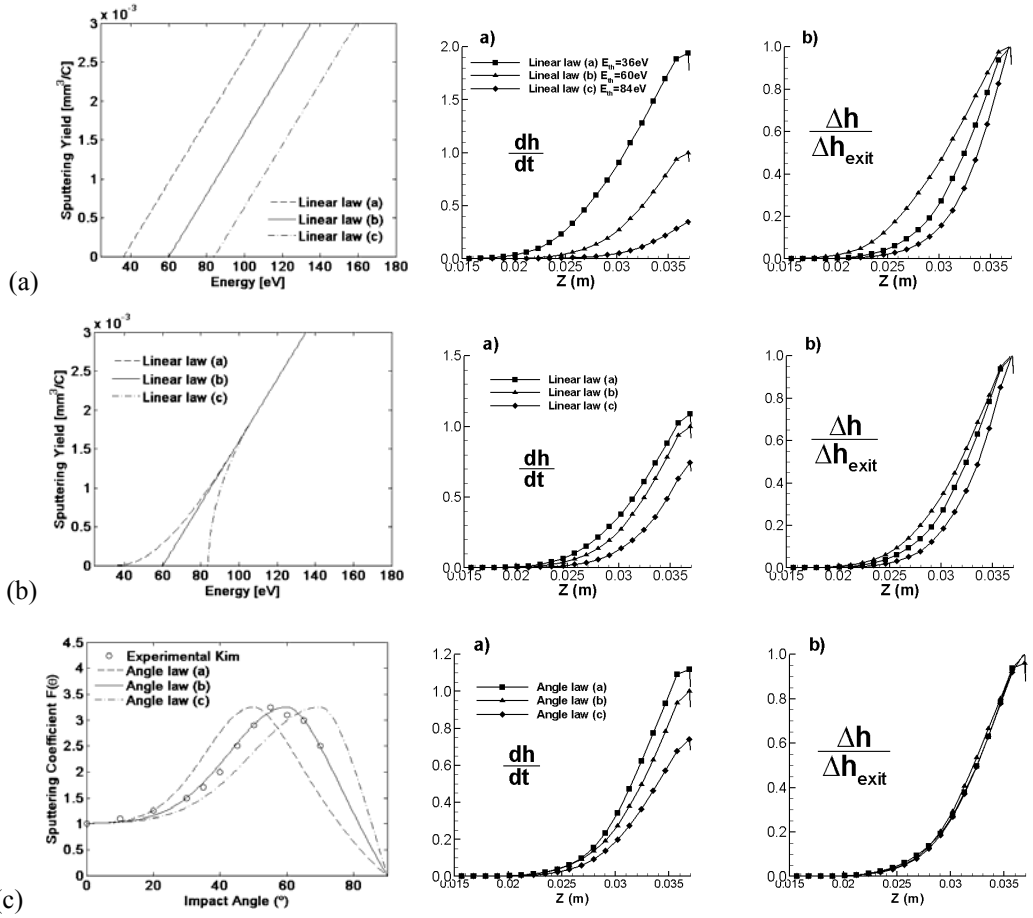

Figure 3: Local erosion rate of the inner wall (for 300V and 6mg/s) for different $Y_V(E,\theta)$: (a) $Y_O(E)$ is depicted in left plot, $F_{\max}$=3 and $\theta_{\max}=60^o$ in $F(\theta)$; (b) $Y_O(E)$ is depicted in left plot, $F_{\max}$ = 3 and $\theta_{\max}=60^o$ were used for $F(\theta)$; (c) $Y_O(E)$ is linear with E_{th}=60eV, $F(\theta)$ is depicted in left plot.

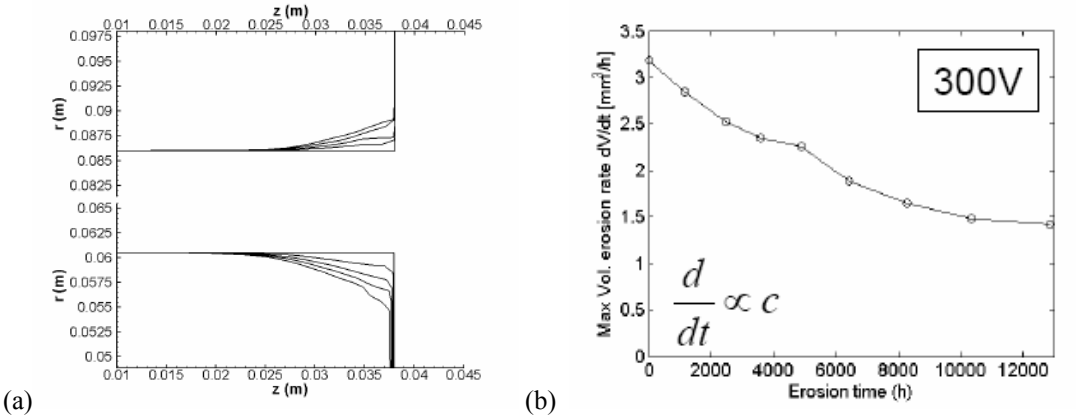

Figure 4: Erosion of the CS5 at 300V and 6mg/s. (a) Chamber walls at different erosion stages. (b) Volumetric erosion rate versus time.

rate with the time of operation; the use of BN, instead of borosil, explains partially that the slope here is smaller than in experiments with SPT-100 and T-220[1,33].

Figure 5 shows the two-dimensional (2D) plasma response at initial and final stages. The widening of the chamber with erosion reduces the plasma density and thus the particle and energy fluxes to the wall. Figure 6(a) shows that the asymmetry between magnitudes at inner and outer walls is significant. Differences on ion fluxes amount to ~100%. They are even larger for fluxes of electron energy, because of the temperature profile, Fig. 5, and the highly non-linear behaviour when Debye sheaths are charge-saturated[3]. Figure 6 (b) plots the decrease of ion fluxes and the erosion rate with time. The different behaviours of q_{iW} and dh/dt are due to the sputtering yield law $Y_V(E,\theta)$.

Figure 7(a) illustrates about the distribution function of energies and incidence angles at 3 different locations of the inner wall at the initial stage. As we move outwards inside the chamber, both the mean ion energy and its dispersion increase and the incidence angle are less perpendicular (we observe that the radial contribution to the ion energy changes mildly along the chamber). The ion energies at the sheath edge indicate that a large part of the axial ion acceleration takes place in the near plume. Sputtering in location 1 is small since the threshold energy is 60 eV. The results of Fig. 7(b) for the last erosion stage show some interesting features. The ion energy in location 3 is significantly larger because of the lower electric potential at Q3. The curvature of the wall leads to less-perpendicular incidence angles, the incidence becoming almost parallel at Q3.

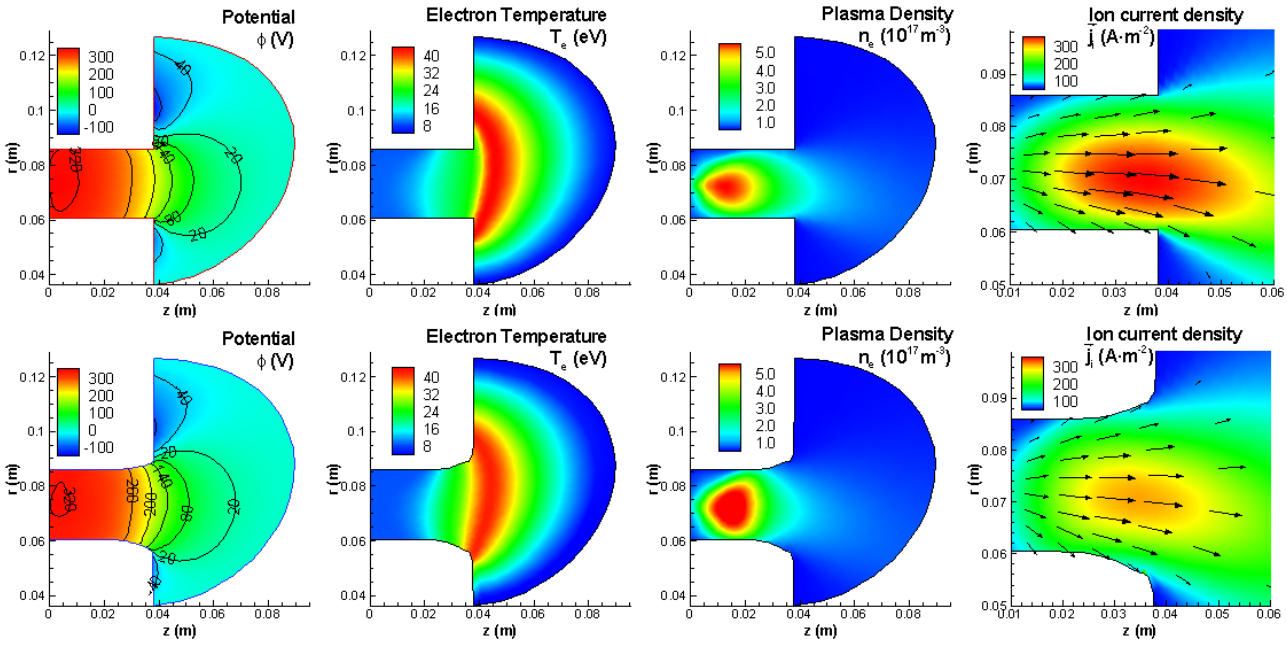

Figure 5: Case 300V and 6mg/s. 2D plasma profiles for stages 0 (up) and 8 (down).

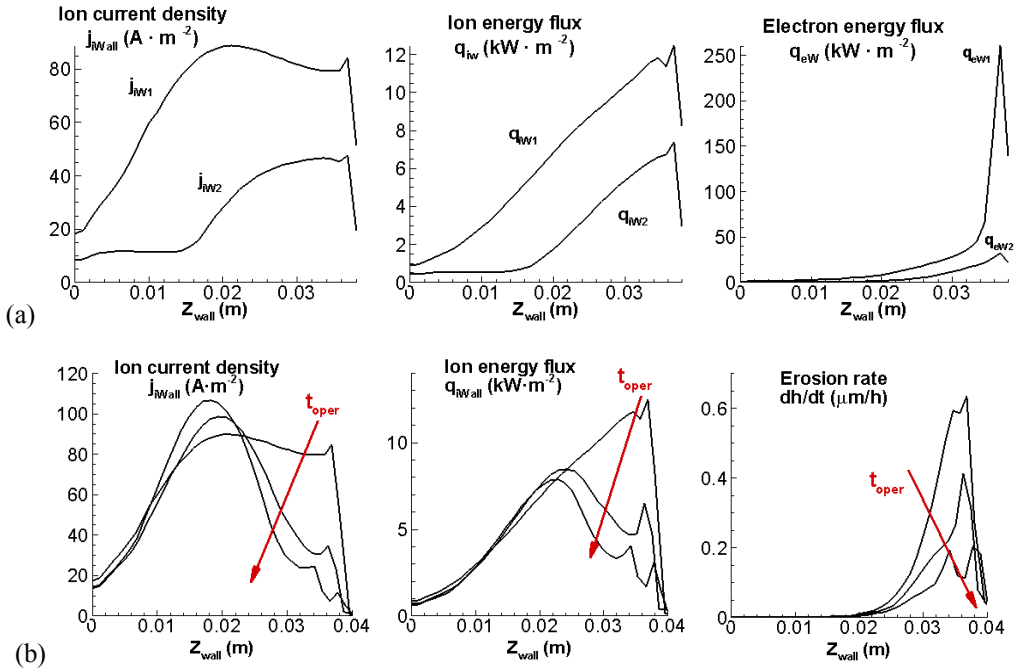

Figure 6: Case 300V and 6mg/s. (a) Comparison of plasma fluxes at inner (1) and outer (2) walls at stage 0. (b) Evolution of fluxes at inner walls at different erosion stages.

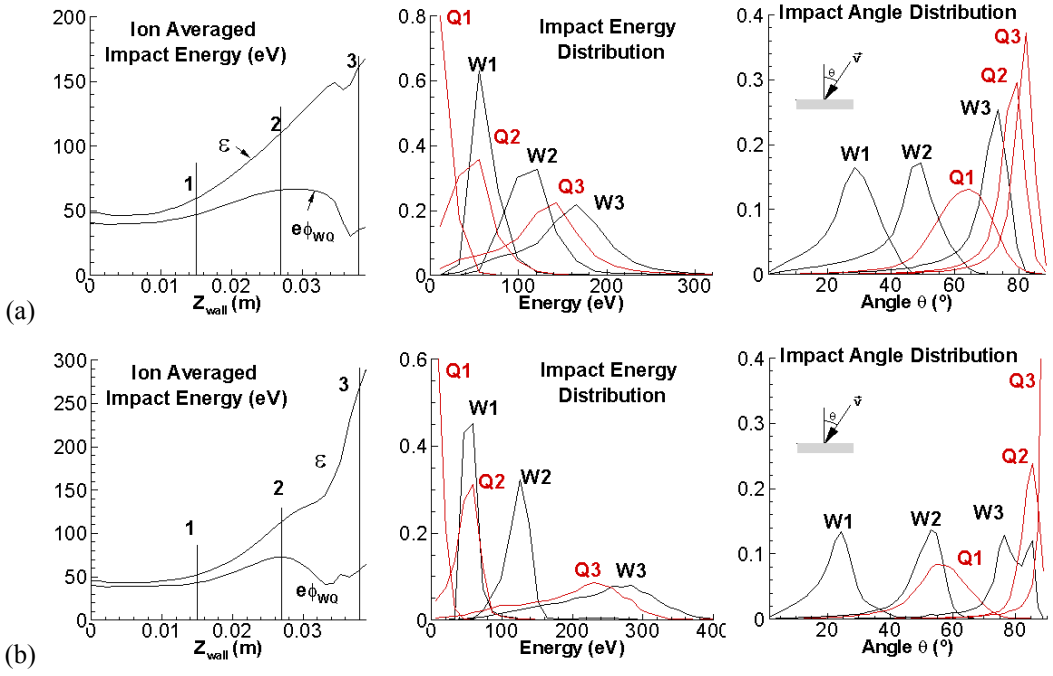

Figure 7: Inner wall magnitudes for 300V and 6mg/s at stages 0 (a) and 8 (b) . (Left) Time-averaged ion energy at the wall E_w and sheath fall ϕ_{WQ}. (Middle) Relative distribution of ion energies E at the 3 radial locations marked in the left plot, at the sheath edge Q and the wall W. (Right) Relative distribution of angles of incidence θ at the same locations. Thruster exit is at location 3.

V. Influence of the discharge voltage

Figures 8 to 11 compare the preceding results for 300V to a simulation with 900V, a 3 times larger magnetic field, and the same mass flow and magnetic field shape (topology B in next Section nomenclature). Erosion is found to be 4-5 times larger for 900V, when a simple estimate from the discharge voltages would suggest a factor slightly above 3. Now, ionization takes place more inwards, which reduces the ion current to the wall: 80 A/m2 for 300V and 60 A/m2 for 900V [Figs. 6(a) and 10], at the inner wall location 3. The lower potential at Q3 and the presence of double ions (~10%) explain the relatively larger energy per ion: 160eV for 300V, and 500eV for 900V [Figs. 9(b) and 10], at the chamber exit. Observe in Fig. 10 that the asymmetry between the ion fluxes at inner and outer walls is larger for 900V than for 300V, which leads to a larger asymmetry in erosion too, Fig. 8(a).

Figure 12 illustrates about the changes on the thruster performances caused by erosion and compares performances for 300V and 900V. For each operation point, erosion modifies slightly the performances. This result, which agrees with experience, is more relevant than the particular trend of performances which is not reliable enough because of the deficiencies and uncertainties on the simulation model.

Incidentally, observe in Fig. 12 that the thruster operates much more efficiently at 900V (and 5kW), with a thrust efficiency of 56-58% [††], thanks mainly to a large increase in current utilization (i.e. the ratio between the ion beam current and the discharge current) from 60% to 78%. This seems natural when we take into account that the thruster was designed to operate at 5kW and not at 2kW.

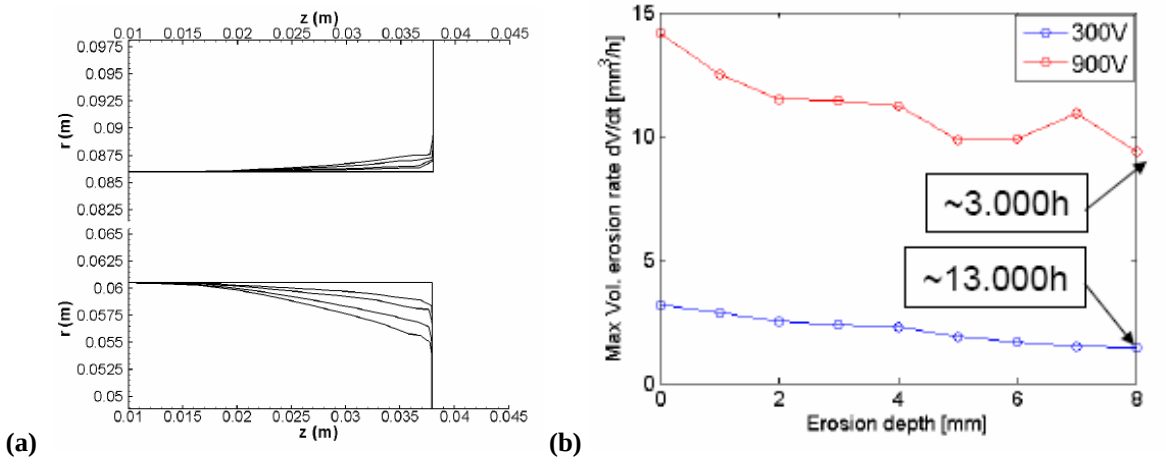

Figure 8: Case 900V and 6mg/s. (a) Wall profiles at different erosion stages. (b) Volumetric erosion rate versus Δh_{exit} for 300V and 900V.

[††] The simulation code underestimates efficiencies always due to a plasma-wall model that overestimates energy losses at ceramic walls.

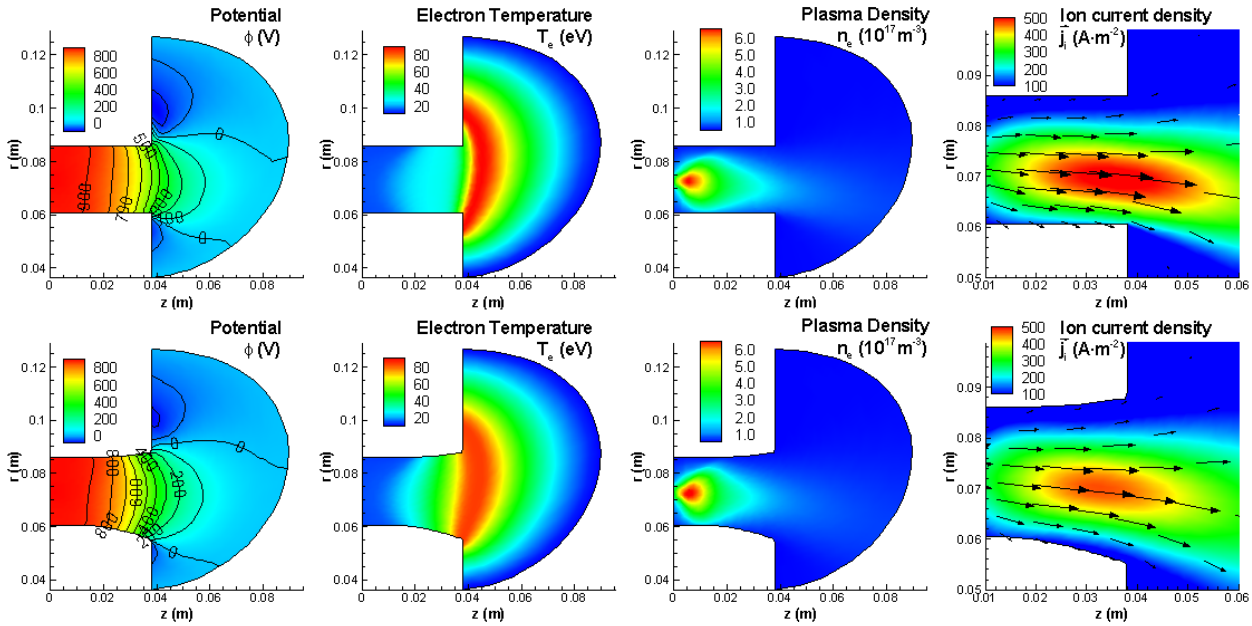

Figure 9: Case 900V and 6mg/s. 2D plasma profiles at erosion stages 0 (up) and 8 (down).

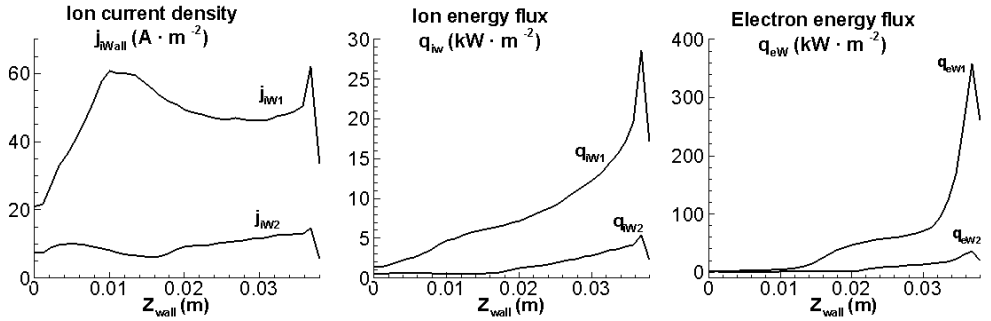

Figure 10: Case 900V and 6mg/s. Plasma fluxes at inner (1) and outer (2) walls at stage 0.

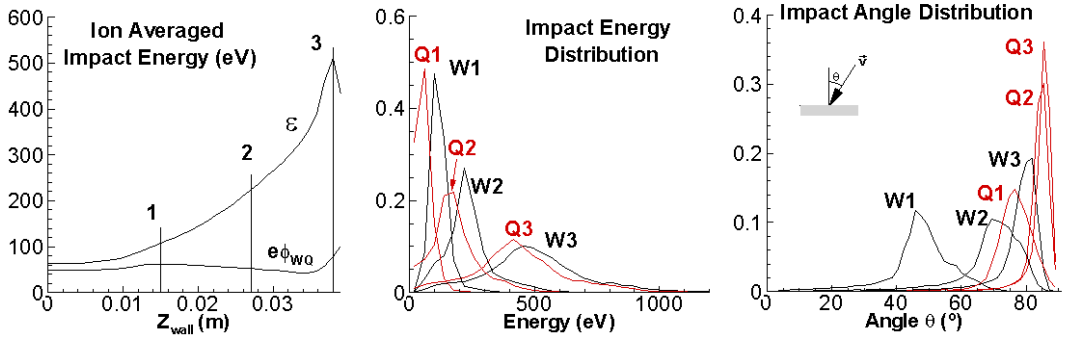

Figure 11: Case 900V and 6mg/s and inner wall. Relative distributions of energies and angles at stage 0.

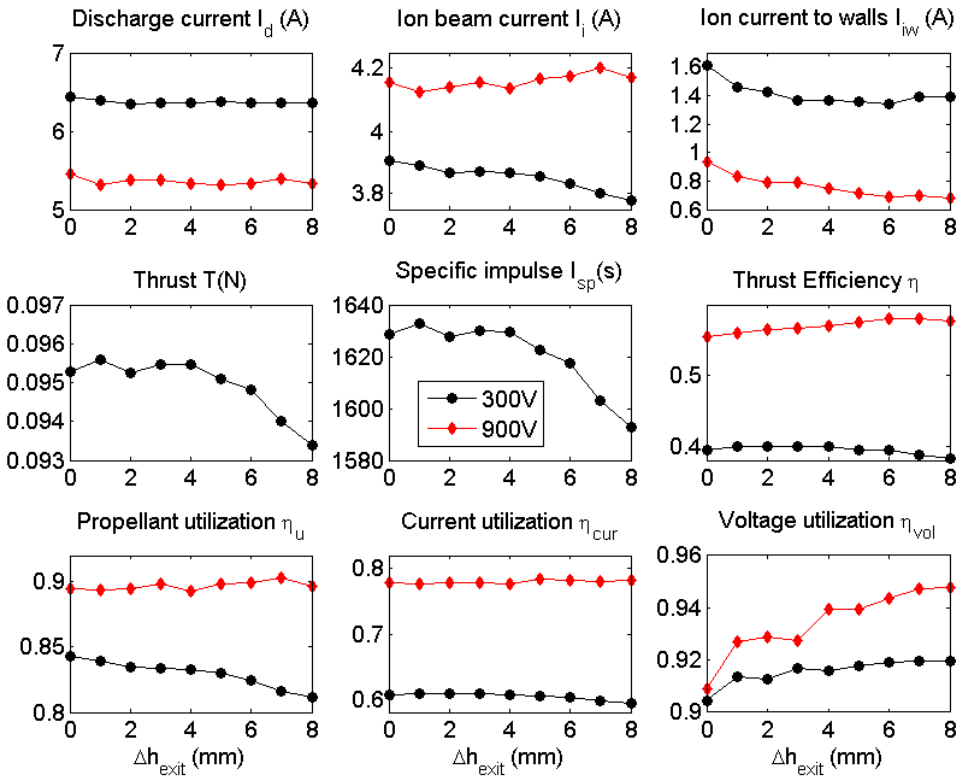

Figure 12: Evolution of thruster performances with erosion for 300V and 900V.

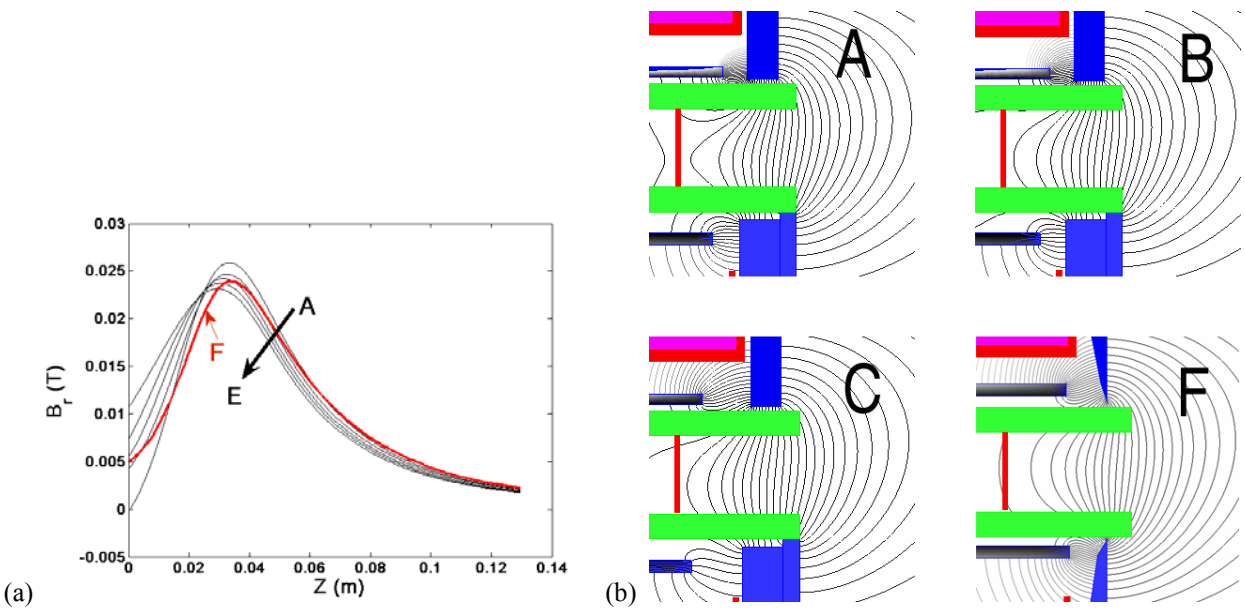

Figure 13: Magnetic topologies used in the simulations. (a) Radial magnetic field at the channel median. (b) 2D topology: the magnetic screens are the horizontal blue lines; the ion core has been modified in topology F.

VI. Influence of the magnetic field topology

Figure 13 depicts the six magnetic field topologies we have used in the simulations. Those for 300V and 900V of the previous sections were run with topology B. The differences between topologies A to E are on the position of the two magnetic screens, followed by a minor correction on the coil currents to adjust the magnetic strength, in order that $\int B_r dz$ in the chamber remains almost constant[26], as Fig. 13 (a) shows. Case F is similar to B but the ion core has been reduced in the tips close to the chamber exit, Fig. 13 (b). This 'exercise' was intended to increase the magnetic lens effect and analyze the effects. The comparison of the magnetic streamlines and equipotential lines for cases B and F, in Fig. 14, shows that the magnetic lens has been effectively increased.

Figure 15 corresponds to operation with topology F and 300V, and must be compared with Fig. 6(a) for topology B and 300V. We observe that the magnetic lens has had a real effect on channelling appropriately the ion fluxes. With topology F, the asymmetry between fluxes at inner and outer walls has been cancelled. The sum of ion energy fluxes to both walls, $q_{iW1} + q_{iW2}$, has not changed much, but the improvement in terms of total erosion are significant. This is because of the erosion rate increases more than linearly with the ion energy flux, so that a levelling between q_{iW1} and q_{iW2} reduces the total erosion. The proof is illustrated in cases B and F of Fig. 16: the erosion to the inner wall is reduced in a 50% with topology F.

Figure 16 also compares the linear erosion Δh_{exit} for cases A to E. The conclusion is that the magnetic topology is a relevant parameter for erosion, which increases about a 30% from A to E. This conclusion is complemented with the comparison of thruster performances for topologies A to E in Fig. 17. Cases A and B are also the best in terms of performances (and possibly also in terms of discharge stability based on dB_r / dz). However, the minimum-erosion topology F leads to a deterioration of performances.

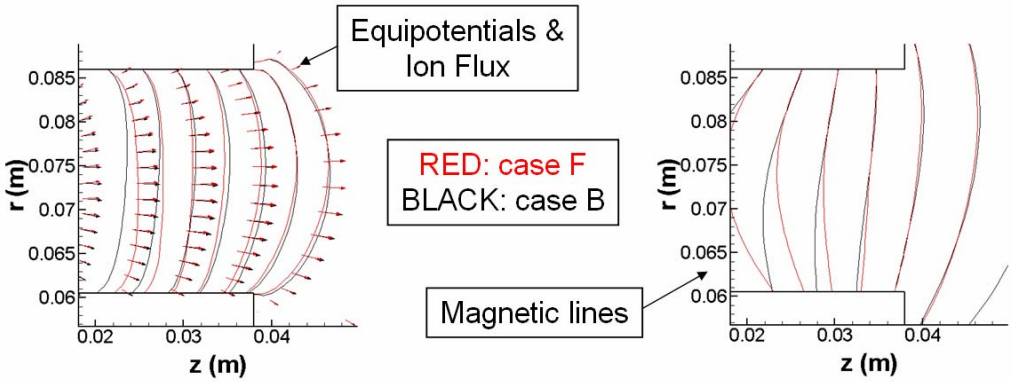

Figure 14: Comparison of magnetic lines and equipotential lines for cases B and F.

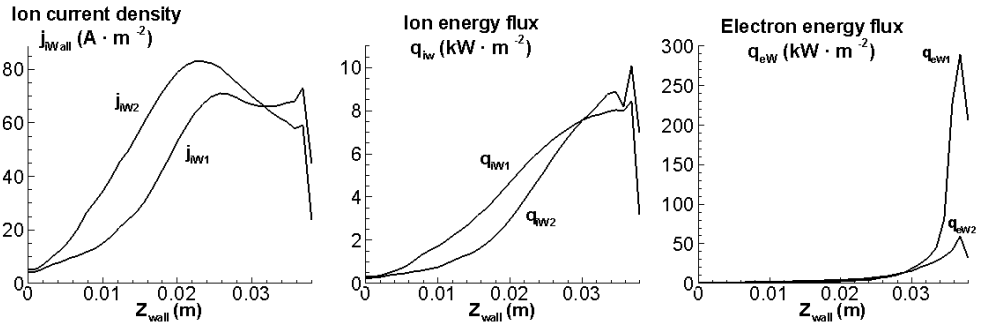

Figure 17: Case 300V, 6 mg/s, topology F. Plasma fluxes at inner (1) and outer (2) walls at stage 0.

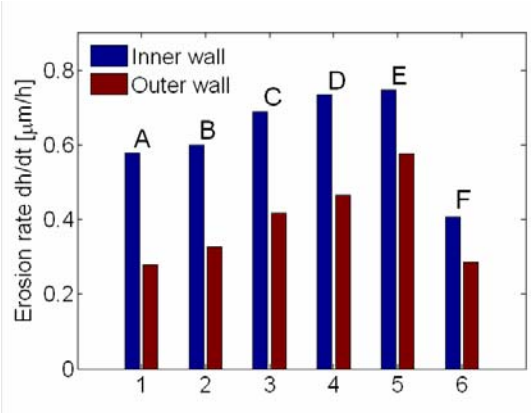

Figure 16: Erosion rate of inner and outer parts of the exit-cross section for different magnetic topologies, 300V, 6 mg/s, and stage 0.

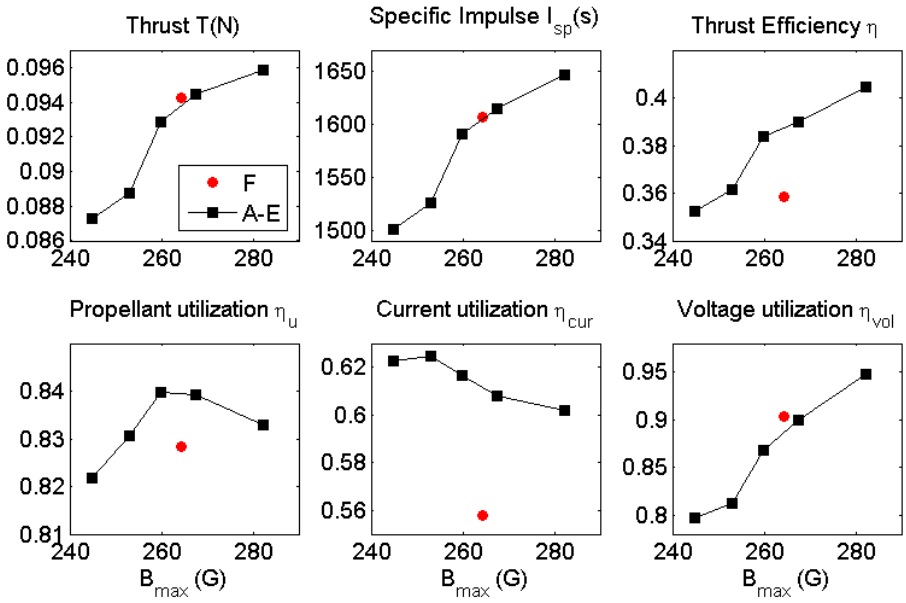

Figure 17: Influence of the magnetic topology in thruster performances, for 300V and 6 mg/s. Blue squares correspond to topologies A to E (from right to left) .

VII. Conclusion

A 2D hybrid code has been used to study wall erosion in Hall thrusters. The method can be very useful since it relates the erosion behavior to the details of the plasma response and to the operation conditions. In particular, it has been shown the influence of the sputtering yield law on the eroded profiles, and the change in erosion trends for high discharge voltages. Also, we have visualized how the increase of the magnetic lens effect can be very effective in reducing energy fluxes to walls and, therefore, erosion.

However, a reliable prediction of wall erosion in Hall thrusters requires significant improvements on both the knowledge of the sputtering yield function and the models implemented in simulation codes of the plasma discharge. More experimental data on the sputtering function (in terms of ion energy and angle and wall temperature) are required because of valid theories (and formulae) of the sputtering process on composite materials at low energies are inexistent. Experiments on the low energy range (<100V) are strongly needed too for moderate discharge voltages (≤300V) .

The state-of-the-art on modeling plasma phenomena in a Hall thruster is not good enough to reproduce accurately the 2D details of the plasma response. The main subjects of incomplete understanding and modeling would be: the amount and evolution of secondary electron emission from the wall[5,38], the distribution function of the weakly-collisional electrons[6,35], and the turbulent diffusion process[11,19]. In addition, numerical algorithms still present limitations on dealing with actual physical conditions, such as the fulfillment of the Bohm condition by the ion current at sheath edges[16] or the 2D solution for magnetized electrons in curved magnetic field topologies[23].

Acknowledgments

This work was financed by contract 19554/05/NL/PA of the European Space Agency. E. Ahedo received support also from project ESP-2004-03093 of the Ministerio de Educación y Ciencia.

Appendix: Fitting experimental data with SRIM simulations

This appendix describes on going work in the simulation of the sputtering process with the SRIM/TRIM program, the calculation of the sputtering yield of different materials (mainly Cu and BN-SiO_2) as a function of the ion energy and incident angle and the fitting to be done between experimental data and simulations predictions.

The SRIM/TRIM code has been used for predicting the sputtering yield of Cu for different incident Xe ions energies and for different angles. The general trend of the simulations is that the sputtering yield of Cu grows with higher incident energies. Also a dependency of the sputtering yield with the incident angle is seen: when the angle separates from normal incidence, the sputtering yields grows up to a maximum which is reached at around 70º – 80º and then a sudden decrease is predicted. This can be seen in the following figure.

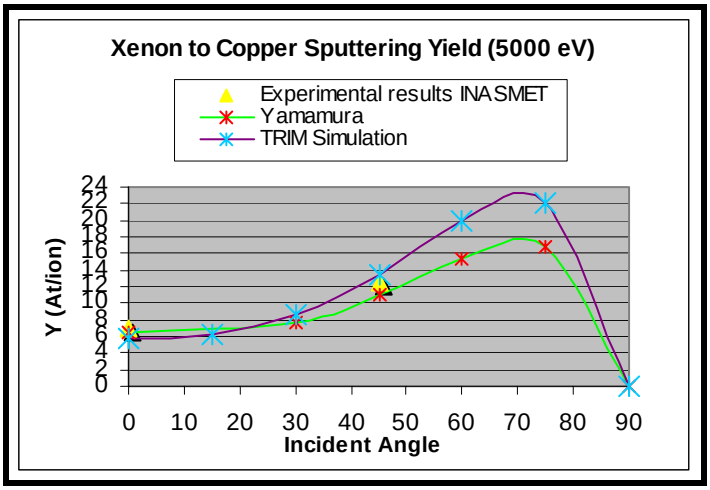

Only limited experimental data obtained at Inasmet are available but, as can be seen in the above figure, these data compare reasonable well with SRIM/TRIM simulations. For an angle of incidence of 0º (normal to the Cu surface) an experimental mean value (two experiments) of 6,84 atm/ion has been obtained, whereas a 5,9 atm/ion has been predicted. For a 45º angle, a mean value (two experiments) of 12,5 atm/ion has been measured whereas a 13,48 atm/ion has been predicted. In order to obtain each experimental value with enough accuracy, the duration of the experiments is quite long (several days), even for the high energies like 5000 eV that have been employed. For lower energies the durations would be measured in weeks.

There has been no problem in comparing the predicted results (obtained in atm/ion) with the measured results (obtained in mm^3/C) as the transformation is quite easy taking into account the Avogrado's number, the density and molar mass of the cupper and the charge of the electron. The key is that the cupper is a monoatomic target.

However, things are rather different for the Borosil (BN-SiO_2), as this is not a monoatomic target. SRIM/TRIM program accepts several elements as components of a layer target, but treats each of them independently, not taking into account binding energies between the different components. The results of the simulations are, in the best case, rough estimations of the real behaviour of the material. Different simulations have been done for several energy levels (in the range present in the HET motors) and values of sputtering yield have been predicted. The general trend is the same that has already been described for cupper: higher incident energies, higher sputtering yields and also a clear dependency with the incident angle, with a maximum around 70º – 80º. However, when trying to compare the predicted results with the experimental data several problems have appeared. First of all, the program predicts an sputtering yield independent for each component (B,N,Si,O). The sputtering yield of the Borosil should be some combination of these values, but this is not complete clear. Several trials have already been done, combining these predicted data, taking also into account the Avogrado's number, the density and molar mass of each component, but not reasonable results have been obtained. Secondly, only very limited experimental data are available at the moment, as the employed energies are lower (500 eV to 1000 eV) than in the cupper's case, and the experiment times are very long. Finally, there has been no opportunity to tune some of the

parameters that affect very much the modelling results (mainly the SBE, Surface Binding Energy) as it is not complete clear the meaning of such parameter in the context of a complex material like the Borosil. More work is needed to solve these problems.

References

1. Abgaryan V., H. Kaufman, V. Kim, V.I. Kozlov, and N.A. Maslennikov, *Calculation analysis of the erosion of the discharge chamber walls and their contamination during prolonged SPT operation*, paper AIAA 94-2859 (1994).
2. Absalamov, S. K. et al., *Measurement of Plasma Parameters in the Stationary Plasma Thruster (SPT-100) Plume and its Effect on Spacecraft Components*, paper AIAA 92-3156 (1992).
3. Ahedo E., *Presheath/sheath model of plasma with secondary emission from two parallel walls,* Physics of Plasmas, vol. 9, pp. 4340-4347 (2002).
4. Ahedo E. and J.M. Gallardo, *Scaling down Hall thrusters*, paper IEPC 03-104 (2003).
5. Ahedo E. and F.I. Parra, *Partial trapping of secondary electron emission in a Hall thruster plasma,* Physics of Plasmas, vol.12, 073503 (2005).
6. Ahedo E. and V. de Pablo, *Combined effects of electron partial thermalization and secondary emission in Hall thruster discharges*, Physics of Plasmas, vol 9, 083501 (2007).
7. Antón A., D. Escobar, and E. Ahedo, *Contour algorithms for a Hall thruster hybrid code*, paper AIAA 2006-4834, (2006).
8. Biagioni L., M. Saverdi, M. Berti, U. Cesari, and M. Andrenucci, *Design and preliminary characterization of a 5 kw Hall thruster prototype*, paper IEPC 03-228 (2003).
9. Boyd I.D. and M.L. Falk, *A Review of Spacecraft Material Sputtering By Hall Thruster Plumes*, paper AIAA 2001-3353 (2006).
10. Britton M., D. Waters, R. Messer, E. Sechkar, and B. Banks, *Sputtering Erosion Measurement on Boron Nitride as a Hall Thruster Material*, NASA /TM 2002-211837 (2002).
11. Cappelli M.A., N. B. Meezan, and N. Gascon, *Transport Physics in Hall Plasma Thrusters,* paper AIAA 2002-0485 (2002).
12. Cheng S. Y., *Modeling of Hall thruster lifetime and erosion mechanisms*, PhD Thesis, MIT (2007).
13. Duchemin O., N. Cornu, F. Darnon, and D. Estublier, *Endurance Test at High Voltage of the PPS X000 Hall-Effect Thruster*, paper AIAA 2005-4050 (2005).
14. Dumazert P., F. Marchandise, N. Cornu, L. Jolivet, and D. Estublier, *PPS-1350-G Qualification Status*, paper AIAA 2004-3604 (2004)
15. Escobar D., A. Antón, and E. Ahedo, *Simulation of high-specific-impulse and double-stage Hall thrusters*, paper IEPC 2005-040 (2005).
16. Escobar D., E. Ahedo, and F. I. Parra., *On conditions at the sheath boundaries of a quasineutral code for Hall thrusters*, paper IEPC 2005-041 (2005).
17. Escobar D. and E. Ahedo, *Improved electron formulation for a Hall thruster hybrid model,* paper AIAA 2006-4326 (2006).
18. Fife J. M., *Hybrid-PIC Modeling and Electrostatic Probe Survey of Hall Thrusters.*, PhD Thesis, MIT (1998).
19. Gallardo J.M. and E. Ahedo, *On the anomalous diffusion mechanism in Hall thrusters,* paper IEPC 2005-117 (2005).
20. Gamero M. and I. Katz, *Estimation of Hall Thruster Erosion Using HPHall*, paper IEPC 2005-303 (2005).
21. Garner C. E., Brophy, J. R., Polk, J. E., and Pless, L. C., *Cyclic Endurance Test of a SPT-100 Stationary Plasma Thruster*, paper AIAA 94-2856 (1994).
22. Garnier Y., V. Viel, J. F. Roussel, and J. Bernard, *Low-Energy Xenon Ion Sputtering of Ceramics Investigated for Stationary Plasma Thrusters*, Journal of Vacuum Science and Technology A, vol, 17, pp. 3246-3254 (1999).
23. Hagelaar G., *Modelling electron transport in magnetized low-temperature discharge plasmas,* Plasma Sources Sci. Technol. vol. 16, pp. S57-S66 (2007).
24. Hippler R., *Fundamental processes in plasma-surface interactions*, in *Low temperature plasma physics*, R. Hippler et al., (editors), Wiley, Berlin (2001).
25. Kannenberg K., V. Khayms, B. Emgushov, L. Werthman, and J. E. Pollard, *Validation of Hall Thruster Plume Sputter Model*, paper AIAA 2001-3986 (2001).
26. Kaufman H.R., *Technology of closed-drift thruster,* AIAA Journal, vol. 23, pp. 78-87 (1985).
27. Kim V., *Main physical features and processes determining the performance of stationary plasma thrusters*, Journal of Propulsion & Power, vol. 14, pp. 736-743 (1998).
28. Kim V., V. Kozlov, A. Semenov, and I. Shkarban, *Investigation of the Boron Nitride based ceramics sputtering yield under its bombardment by Xe and Kr ions*, paper IEPC 01-073 (2001).
29. Kim V., V. Kozlov, V. Skrylnikov, N. Hilleret, B. Henrist, S. Locke, and M. Fife, *Investigation of operation and characteristics of small SPT with discharge chamber walls made of different ceramics*, paper AIAA 2003-5002 (2003).

30. Kim V., V. Abgaryan, V. Kozlov, and V. Skrylnikov, *Development of the accelerated test procedure for the SPT discharge chamber wall wearing during long thruster operation*, paper AIAA 2003-5003 (2003).
31. Lovtsov A.S., A.A. Shagayda, and O.A. Gorshkov, *Semi-Empirical Method of Hall Thrusters Lifetime Prediction*, paper AIAA 2006-4661 (2006).
32. Limburg, *Sputter Theory and Data for Ion Engines*, STR-258, ESA, Noordwijk, The Netherlands (1998).
33. Mason L.S., R.S. Jankovsky, and D.H. Manzella, *1000 hours of testing on a 10 kilowatt Hall effect thruster*, paper AIAA 2001-3773 (2001).
34. Mazouffre, S., F. Dubois, L. Albarede, D. Pagnon, M. Touzeau, M. Dudeck, *Plasma induced erosion phenomena in a Hall thruster*, Proc. on Intern. Conf. on Recent Advances in Space Technologies (2003).
35. Meezan N. B. and M.A. Capelli, *Kinetic study of wall collisions in a coaxial Hall discharge,* Physical Review E, vol. 66, 036401 (2002).
36. Parra F.I., E. Ahedo, M. Fife, and M. Martínez-Sánchez, *A two-dimensional hybrid model of the Hall thruster discharge*, Journal of Applied Physics, vol. 100, 023304 (2006).
37. Peterson P.Y. and D.H. Manzella, *Investigation of the erosion characteristics of a laboratory Hall thruster*, paper AIAA 2003-5005 (2003).
38. Sydorenko D., A. Smolyakov, I. Kaganovich, and Y. Raitses, *Kinetic simulation of secondary electron emission effects in Hall thrusters,* Physics of Plasmas, vol. 13, 014501 (2006).
39. Yamamura Y., *An Empirical formula for angular dependence of sputtering yields*, Radiation Effects, vol. 80, pp. 57-72 (1984).
40. Yamamura Y. and H. Tawara, *Energy Dependence of Ion-Induced Sputtering Yields from Monatomic Solids at Normal Incidence*, Atomic Data and Nuclear Data Tables, vol. 62, pp. 149-253 (1996).